

Electromagnetically Induced Transparency of Interacting Rydberg Atoms with Two-Body dephasing

Dong Yan,^{1, 2,*} Binbin Wang,¹ Zhengyang Bai,^{2, 3} and Weibin Li^{2, †}

¹*School of Science and Key Laboratory of Materials Design and Quantum Simulation, Changchun University, Changchun 130022, P. R. China*

²*School of Physics and Astronomy, University of Nottingham, Nottingham, NG7 2RD, United Kingdom*

³*State Key Laboratory of Precision Spectroscopy, East China Normal University, Shanghai 200062, P. R. China*

(Dated: December 15, 2024)

We study electromagnetically induced transparency of a ladder type configuration in ultracold atomic gases, where the upper level is an electronically highly excited Rydberg state. We study a scenario where both dispersive and dissipative long-range interactions between Rydberg atoms are present. This is motivated by recent experimental discovery, where molecular transitions cause an effective two-body dephasing process. It has been shown that long-range van der Waals interactions suppress simultaneous excitations of multiple Rydberg atoms within a blockade volume. We show that the nonlocal, two-body dissipative process enhances the excitation blockade. Through numerical and approximately analytical calculations, we show that transmission of the probe field is reduced drastically in the transparent window, which is accompanied by stronger photon-photon anti-bunching. Around the Autler-Townes splitting, photon bunching is amplified by the two-body dephasing, while the transmission is largely unaffected.

PACS numbers:

I. INTRODUCTION

Electromagnetically induced transparency (EIT) plays a pivotal role in quantum and nonlinear optics and has been investigated intensively in the past two decades as a typical example of coherent interference effects [1–3]. EIT finds applications in slowing down light speed and even storing light as atomic excitations [4–8], preparing quantum entangled states [9, 10], implementing logic operation for quantum information processing and optical communication [11, 12]. Recently it has been shown that strong and long-range interactions between individual photons can be achieved using Rydberg atoms, which are in electronically highly excited states with principal quantum number $n \gg 1$. Rydberg atoms have long life times ($\sim n^3$) and strong interactions (e. g. van der Waals interaction strength $\sim n^{11}$). Such strong interaction changes energies of spatially separated Rydberg atom pairs stat. Hence a Rydberg atom strongly suppresses Rydberg excitation of nearby atoms, giving rise to the so-called excitation blockade effect. The strong Rydberg atom interaction can be mapped to light fields at the few-photon level through EIT [13, 14]. This allows us to study nonlinear quantum optics [15] and find potential applications in quantum information processing, such as single photon generation [16–18], single-photon filters [13, 19], single-photon substractors [20, 21], single-photon transistors [22, 23], single-photon switches [24, 25], single-photon gates [26, 27], and

photonic dimers and trimers [28, 29].

Experimentally Rydberg states with low angular momentum quantum numbers, such as S -, P - and D - states can be excited through single or two photon excitations [30]. The rich Rydberg levels have permitted experimental and theoretical investigations of EIT with single [31–49] as well as multiple components Rydberg states [50–56]. In cases of Rydberg S - and P -states, large energy spacing (compared to laser Rydberg frequencies) between neighboring Rydberg states leads to coherent two-body interactions, which lay the foundation for many optical quantum information applications [30].

Dephasing and decay of Rydberg atoms are unavoidable in long time dynamics due to, e.g., atomic motions and finite lasers linewidth [57]. In this situation, dynamics of Rydberg gases are modelled by open quantum systems. Competitions between dissipation of individual atoms and two-body Rydberg interactions as well as laser-atom coupling results to interesting driven-dissipative many-body dynamics, such as glassy dynamics induced by dephasing of single Rydberg atoms in a lattice system [58], bistability and metastability [59], Mott-superfluid phase transition [60], emergence of anti-ferromagnetic phases [61], dissipation controlled excitation statistics [62], and dissipation induced blockade and anti-blockade effects [63].

While previous studies have focused on incoherent channels at single Rydberg atoms, two body dissipation occurs in dense atomic ensembles. For example, collective decay of Rydberg atoms is generated by strong atom-background photon field coupling. The resulting superradiance considerably increases decay rate of Rydberg atoms on top of single atom decay [64, 65]. A recent experiment demonstrated that transmission of a weak

*Electronic address: ydbest@126.com

†Electronic address: weibin.li@nottingham.com

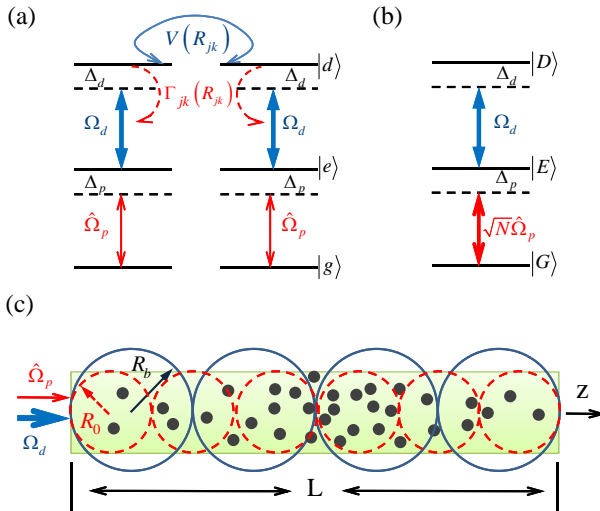


FIG. 1: (Color online) (a):Level scheme. Cold atoms are driven by a classical coupling field (with Rabi frequency Ω_d and detuning Δ_d) and a weak probe field (Rabi frequency $\hat{\Omega}_p$ and detuning Δ_p) in a three-level ladder configuration where $|g\rangle$, $|e\rangle$ and $|d\rangle$ are ground state, intermediately excited state and highly excited Rydberg state, respectively. $V(R_{jk})$ and $\Gamma_{jk}(R_{jk})$ are long-range van der Waals interaction potential and two-body dephasing, which depend on space separation R_{jk} between two atoms. (b) An equivalent level structure for a superatom (SA) which is composed of three collective state $|G\rangle$, $|E\rangle$ and $|D\rangle$ regardless of the shape of the SA in the weak-probe limit. Note that in this case the probe Rabi frequency is enhanced by a factor of $\sqrt{N_a}$ with number of atoms N_a . (c) Geometrical arrangements of the SAs with (blue solid line) and without (red dashed line) TBD in the presence of vdW interactions when the weak probe field propagates in an one-dimensional atomic ensemble. The sphere represents areas of SAs.

probe field in a cold gas of Rubidium atoms excited to Rydberg D -states decreases slowly with time [66]. Such non-equilibrium transmission is attributed to the fact that two Rydberg atoms in the target D -states couple to energetically close pair states. It was argued that the molecular vibration-Rydberg state coupling opens a two-body dephasing (TBD) channel [66]. Note that collective dephasing was predicted to occur between quantum emitters (two-level atoms), which is originated from spin-phonon coupling [67].

In this work, we study Rydberg-EIT in a regime where spatially dependent dephasing between Rydberg atoms is relevant. In our model, both the *interactions* and *dissipations* of Rydberg atoms depend on separations between Rydberg atoms. Using an effective superatom (SA) model [49], we study the interplay between coherent and incoherent two-body processes. We find that the blockade radius is enlarged by the presence of two-body dephasing. As a consequence, this alters transmission

and two-body correlation of the probe field.

The structure of the work is the follows. In Sec. II, the Hamiltonian of the system is introduced. A many-body master equation is used to describe the dissipative dynamics. In Sec. III, the approximate method to solve light propagation and atomic dynamics is introduced. In Sec. IV, we present main results of this work, namely transmission of the probe field. We identify parameter regions where the transmission is affected most. In Sec. V, we will show how photon-photon correlations are modified by TBD. Through numerical and analytical calculations, we determine scalings of the blockade radius with respect to the two-body interactions. We conclude in Sec. IV.

II. MASTER EQUATION OF THE MANY-ATOM SYSTEM

We consider a cold gas of N_a Rb atoms, which are described by a three-level ladder type configuration with a long-lived ground state $|g\rangle$, a low-lying excited state $|e\rangle$ with decay rate γ_e , and a highly excited Rydberg state $|d\rangle$. The level scheme is shown in Fig.1(a). For Rb atoms [66], for example, these states are given by $|g\rangle = |5S\rangle$, $|e\rangle = |5P\rangle$ and $|d\rangle = |nD\rangle$. The upper transition $|e\rangle \rightarrow |d\rangle$ is driven by a classical control field with Rabi frequency Ω_d and detuning Δ_d . The lower transition $|g\rangle \rightarrow |e\rangle$ is coupled by a weak laser field, whose electric field operator and detuning is given by $\hat{\mathcal{E}}_p$ and Δ_p , respectively. In Rydberg states, two atoms located at \mathbf{r}_j and \mathbf{r}_k will experience long-range interactions. Here we assume this is a van der Waals (vdW) type interaction, given by $V(R_{jk}) = \hbar C_6/R_{jk}^6$, where C_6 is the dispersion coefficient and $R_{jk} = |\mathbf{r}_j - \mathbf{r}_k|$ is the distance between the two atoms. The Hamiltonian of the system reads

$$\hat{H} = \hat{H}_0 + \hat{V}_d(R), \quad (1)$$

where $\hat{H}_0 = \sum_j [\Delta_p \hat{\sigma}_j^{ee} + (\Delta_p + \Delta_d) \hat{\sigma}_j^{dd}] + [\hat{\Omega}_p \hat{\sigma}_j^{eg} + \Omega_d \hat{\sigma}_j^{ed} + \text{H.c.}]$ describes the atom-light interaction. We have defined the Rabi frequency operator $\hat{\Omega}_p = g \hat{\mathcal{E}}_p$ with g the single atom coupling constant [57]. $\hat{V}_d(R) = \sum_{j>k} V(R_{jk}) \hat{\sigma}_j^{dd} \hat{\sigma}_k^{dd}$ is the vdW interaction between Rydberg atoms. Here $\hat{\sigma}_j^{mn} = |m\rangle_j \langle n|$ is the projection operator of the j -th atom. Taking into account dissipative processes, dynamics of the many-atom system is governed by the following master equation

$$\begin{aligned} \dot{\rho} = & -i[\hat{H}, \rho] + 2\gamma_e \sum_j [\hat{\sigma}_j^{ge} \rho \hat{\sigma}_j^{eg} - \frac{1}{2} \{\rho, \hat{\sigma}_j^{eg} \hat{\sigma}_j^{ge}\}] \\ & + 2\gamma_d \sum_j [\hat{\sigma}_j^{dd} \rho \hat{\sigma}_j^{dd} - \frac{1}{2} \{\rho, \hat{\sigma}_j^{dd}\}] \\ & + \sum_{j>k} \Gamma_{jk} \left[\hat{\sigma}_j^{dd} \hat{\sigma}_k^{dd} \rho \hat{\sigma}_k^{dd} \hat{\sigma}_j^{dd} - \frac{1}{2} \{\rho, \hat{\sigma}_k^{dd} \hat{\sigma}_j^{dd}\} \right], \quad (2) \end{aligned}$$

where γ_d is single atom dephasing rate in state $|d\rangle$. $\hat{\Gamma}_{jk}$ gives the two-atom dephasing rate [66, 67]. To be concrete we assume $\hat{\Gamma}_{jk}$ has a similar spatial dependence as the vdW interaction, i.e., $\Gamma_{jk} = \hbar\Gamma_6/R_{jk}^6$ with Γ_6 being a coefficient characterising the strength of the TBD.

Without TBD, isotropic van der Waals interactions between atoms give rise to an excitation blockade effect [32, 33, 36, 37, 41, 49, 52, 68] within a sphere $V_0 = 4\pi R_0^3/3$. In this volume, a single Rydberg excitation lifts the resonance condition of other atoms. The volume is determined by the blockade radius $R_0 \simeq \sqrt[6]{C_6\gamma_e/\Omega_d^2}$ [49]. When density ρ of atomic gases is high, $N_a = \rho V_0 > 1$ atoms share one Rydberg excitation, which permits us to introduce the so called superatom model for such collective single Rydberg excitation [36, 37, 41, 49, 52, 68]. Within the blockade volume, a superatom has three collective states, the ground state $|G\rangle = |g_1, \dots, g_{N_a}\rangle$, singly excited states $|E\rangle = \sum_j |g_1, \dots, e_j, \dots, g_{N_a}\rangle/\sqrt{N_a}$ and $|D\rangle = \sum_j |g, \dots, d_j, \dots, g_{N_a}\rangle/\sqrt{N_a}$. Other states are prohibited from the dynamics in the weak-probe field limit. A very important consequence of the formation of superatoms is that most atoms behave like two-level atoms. This breaks the EIT condition and causes light scattering. Note that the blockade volume is not always spherical symmetry. Other shapes could be obtained if the van der Waals interaction is spatially anisotropic [69].

When the TBD is present, the blockade volume will be increased. To illustrate this, we write down the non-Hermitian effective Hamiltonian of the master equation [70],

$$\hat{H}_{eff} = \hat{H}_0 + \hbar \sum_{j>k} \left(\frac{C_6}{R_{jk}^6} - i \frac{\Gamma_6}{2R_{jk}^6} \right) \hat{\sigma}_j^{dd} \hat{\sigma}_k^{dd}, \quad (3)$$

we have written the coherent and incoherent two-body terms together. Under resonance condition $\Delta_p = \Delta_d = 0$, we can derive a new, combined blockade radius by comparing the two-body and laser coupling part of the effective Hamiltonian,

$$R_b \simeq \sqrt[6]{\left| 1 - i \frac{\Gamma_6}{2C_6} \right|} \cdot R_0 \quad (4)$$

This result shows that the bigger the value Γ_6 , the larger the combined blockade radius R_b is. At the limit $\Gamma_6 \gg C_6$, the blockade radius $R_b \sim \sqrt[6]{\Gamma_6/C_6} R_0$. A direct consequence of a larger blockade radius is that more atoms are blocked from Rydberg excitations, which reduces the transmission signal of the probe light.

III. HEISENBERG-LANGEVIN EQUATIONS OF THE LIGHT PROPAGATION

In this section, we will study how the van der Waals interactions and TBD together affects light propagation

in the atomic gas. In general, it is difficult to calculate directly responses of light fields in the presence of two-body interactions. In our case, the situation is even complicated as the vdW interaction and the TBD are coherent and incoherent two-body coupling, respectively. With the help of the blockade radius in Eq. (4), this allows us to study light propagation by employing the so-called superatom model [49]. We will work in the continuous limit, i.e. high atomic densities, and focus on one dimensional geometry, which is a good approximation as widths of light pulses are assumed to be smaller than the traversal extension of the atomic gas.

With these approximations and starting from the master equation (2) we obtain Heisenberg-Langevin equations of the operators in the weak-probe limit [49]

$$\begin{aligned} \partial_t \hat{\mathcal{E}}_p(z) &= -c\partial_z \hat{\mathcal{E}}_p(z) + i\eta N \hat{\sigma}_{ge}(z), \\ \partial_t \hat{\sigma}_{ge}(z) &= -(i\Delta_p + \gamma_e) \hat{\sigma}_{ge}(z) - i\Omega_p^\dagger(z) - i\Omega_d \hat{\sigma}_{gd}(z), \\ \partial_t \hat{\sigma}_{gd}(z) &= -i \left[\Delta + \hat{S}_V(z) - i\hat{S}_\Gamma(z) \right] \hat{\sigma}_{gd}(z) \\ &\quad - \gamma_d \hat{\sigma}_{gd}(z) - i\Omega_d \hat{\sigma}_{ge}(z), \end{aligned} \quad (5)$$

where $\Delta = \Delta_p + \Delta_d$ is two-photon detuning. $\hat{S}_V(z) = \int d^3 z' \rho(z') C_6/|z - z'|^6 \hat{\sigma}_{rr}(z')$ and $\hat{S}_\Gamma(z) = \int d^3 z' \rho(z') C_6'/2|z - z'|^6 \hat{\sigma}_{rr}(z')$ are spatially dependent interaction energy and TBD rate, respectively. Both of \hat{S}_V and \hat{S}_Γ are nonlocal in the sense that these local quantities depend on overall atomic density $\rho(z)$ and excitation probability distribution $\hat{\sigma}_{rr}(z)$.

Following the procedure in Ref. [49], we solve the Heisenberg-Langevin equations of independent SAs in the steady state and obtain the Rydberg excitation projection operator

$$\hat{\Sigma}_{dd}(z) = \frac{N_a \eta^2 \hat{\mathcal{E}}_p^\dagger(z) \hat{\mathcal{E}}_p(z) \Omega_d^2}{N_a \eta^2 \hat{\mathcal{E}}_p^\dagger(z) \hat{\mathcal{E}}_p(z) \Omega_d^2 + (\Omega_d^2 - \Delta \Delta_p)^2 + \Delta^2 \gamma_e^2}. \quad (6)$$

The polarizability of the probe field is conditioned on the projection,

$$\hat{P}(z) = \hat{\Sigma}_{dd}(z) P_2 + \left[1 - \hat{\Sigma}_{dd}(z) \right] P_3 \quad (7)$$

where the polarizability becomes that of two-level atoms in a SA

$$P_2 = \frac{i\gamma_e}{\gamma_e + i\Delta_p} \quad (8)$$

and that of three-level atoms otherwise

$$P_3 = \frac{i\gamma_e}{\gamma_e + i\Delta_p + \frac{\Omega_d^2}{\gamma_d + i\Delta}}. \quad (9)$$

It is clearly that optical response of a SA depends on the Rydberg projection (6), i.e., SAs behave like a two-level, absorptive medium due to $\hat{\Sigma}_{dd}(z) = 1$.

The transmission of the probe light is captured by the probe light intensity $I_p(z) = \langle \hat{\mathcal{E}}_p^\dagger(z) \hat{\mathcal{E}}_p(z) \rangle$. In the steady

state, the intensity $I_p(z)$ satisfies a first order differential equation,

$$\partial_z \langle \hat{\mathcal{E}}_p^\dagger(z) \hat{\mathcal{E}}_p(z) \rangle = -\kappa(z) \langle \text{Im}[\hat{P}(z)] \hat{\mathcal{E}}_p^\dagger(z) \hat{\mathcal{E}}_p(z) \rangle, \quad (10)$$

where $\kappa(z) = \rho(z) \omega_p / (\hbar \epsilon_0 c \gamma_e)$ denotes the resonant absorption coefficient. Similarly we find the two-photon correlation function $g_p(z) = \langle \hat{\mathcal{E}}_p^{\dagger 2}(z) \hat{\mathcal{E}}_p^2(z) \rangle / \langle \hat{\mathcal{E}}_p^\dagger(z) \hat{\mathcal{E}}_p(z) \rangle^2$ obeys [49]

$$\partial_z g_p(z) = -\kappa(z) \text{Im}[P_2 - P_3] \langle \hat{\Sigma}_{rr}(z) \rangle g_p(z). \quad (11)$$

The blockade radius is encoded in the correlation function of photon pairs, which decays with the rate proportional to the excitation probability $\langle \hat{\Sigma}_{RR} \rangle$ and absorption rate of a two-level atom when photon separation is smaller than the blockade radius.

Following Ref. [49], we solve Eq. (5)-(11) with a stochastic procedure. Specifically, the 1D atomic medium is divided into $N_{SA} = L / (2R_b)$ superatoms, and then we judge Rydberg excitation whether $\langle \hat{\Sigma}_{rr}(z) \rangle \rightarrow 1$ or $\langle \hat{\Sigma}_{rr}(z) \rangle \rightarrow 0$ in each SA one by one until the last one via a Monte Carlo sampling. We then average many independent realizations to evaluate mean values.

IV. TRANSMISSION OF THE PROBE FIELD

In this section, we will study the influence of the TBD on the transmission of the probe field, which is characterized by the ratio of light intensities at the output and input, i.e. $\tilde{I}_p(L) = I_p(L) / I_p(0)$ with input values $I_p(0)$. In conventional EIT, the transmission varies with the probe field detuning. High transmission is obtained in the EIT window, $|\Delta_p| \leq |\Omega_d|^2 / \gamma_e$ [3]. When turning on the TBD ($\Gamma_6 > 0$), it is apparently the transmission is suppressed in the EIT window, see Fig. 2a. Increasing the strength Γ_6 of the TBD, the transmission $\tilde{I}_p(L)$ decreases gradually (Fig. 2b). A weaker transmission indicates that there are more atoms blocked from forming dark state polariton [3]. One can understand this by analysing blockade radius R_b . When Γ_6 is increased, the blockade radius becomes larger, see Eq. (4). Fixing atomic densities, more atoms behave similar to two-level atoms in the blockade volume. We will discuss in detail the relation between blockade radii and rate Γ_6 in the following section.

Outside the EIT window $|\Delta_p| > \Omega_p$, the transmission first decreases with increasing detuning Δ_p . It arrives at the minimal transmission around the Autler-Townes splitting $\Delta_p = \pm \Omega_d$. In this region, the TBD is less important, and the transmission is almost identical to cases when $\Gamma_6 = 0$ (Fig. 2a). Similar to transmission of EIT in a Rydberg medium [49], the medium enters a linear absorption regimes, where neither vdW interactions nor TBD affect photon absorption dramatically.

In the following, we will focus on the transmission in the EIT window and explore how the TBD interplays

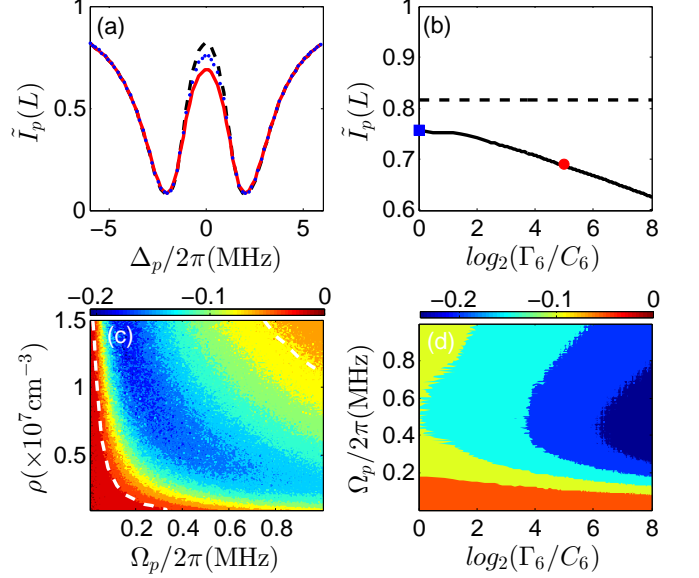


FIG. 2: (Color online) (a) Transmission versus the probe field detuning Δ_p/π for TBD rate $\Gamma_6 = 0$ (dashed), $\Gamma_6 = C_6$ (dotted) and $\Gamma_6 = 32C_6$ (solid). (b) Dependence of the transmission on the TBD rate Γ_6 at the EIT resonance. The square and circle denote values of the transmission in (a) when $\Delta_p = 0$. (c) Transmission as a function of Rabi frequency Ω_p and atomic density ρ . A TBD active region is found when $|\delta \tilde{I}_p(L)| > 1\%$. The probe detuning $\Delta_p = 0$. (d) Transmission as a function of TBD rate Γ_6 and Rabi frequency Ω_p . Increasing Γ_6 and Ω_p will reduce the probe field transmission. The latter is caused by stronger blockade effect due to vdW density-density interactions. In panels (a), (b) and (d), the atomic density is $\rho = 0.5 \times 10^{11} \text{ mm}^{-3}$. Rabi frequency $\Omega_p(0)/2\pi = 0.3 \text{ MHz}$ in (a) and (b). $\Gamma_6 = 32C_6$ in panel (c). Other parameters are $\Omega_d/2\pi = 2.0 \text{ MHz}$, $\Delta_d/2\pi = 0.0 \text{ MHz}$, $\gamma_e/2\pi = 3.0 \text{ MHz}$, $\gamma_d/2\pi = 10.0 \text{ kHz}$, $C_6/2\pi = 1.4 \times 10^{11} \text{ s}^{-1} \mu\text{m}^6$, and $L = 1.0 \text{ mm}$.

with other parameters. We first calculate the transmission by varying atomic density and probe field Rabi frequency. To highlight effects due to the TBD, we calculate differences of the transmission with and without TBD, $\delta \tilde{I} = \tilde{I}_p(L) - \tilde{I}_p^0(L)$ where $\tilde{I}_p^0(L)$ denotes the light transmission when the TBD is turned off. The result is shown in Fig. 2c. We find that stronger probe field (larger Ω_p) and higher atomic densities in general lead to more pronounced TBD effect. In Fig. 2c, we plot a ‘phase diagram’ to distinguish TBD dominated regions. To do so, we plot a phase boundary (dashed curve) when the difference $\delta \tilde{I} > 1\%$. Below this curve the transmission is largely affected by the vdW interactions while above this curve, the atomic gas exhibits active TBD phase, where the transmission is reduced. In Fig. 2d, we show the transmission by varying both the Rabi frequency Ω_p and TBD rate Γ_6 . Fixing Γ_6 , the transmission decreases with increasing Ω_p . This is a result of the Rydberg blockade

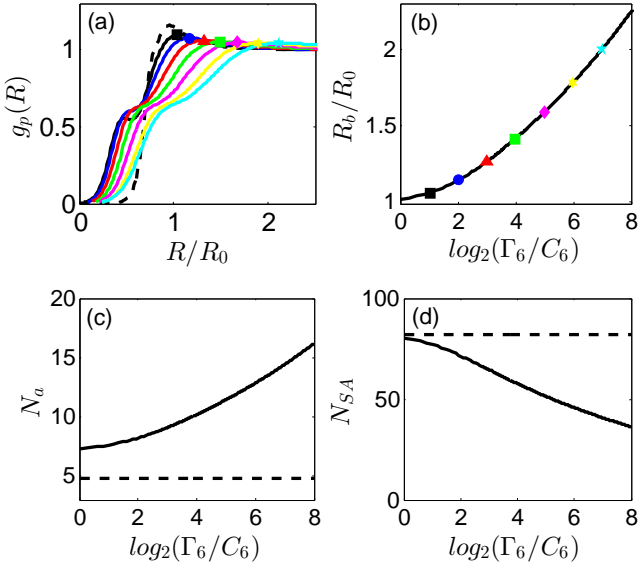


FIG. 3: (Color online) (a) Second-order correlation function $g_p(R)$. Increasing the TBD rate Γ_6 , values of $g_p(R)$ reduce gradually. The maximal value of the correlation usually occurs at the effective blockade radius when the single-photon transition is slightly detuned ($\Delta_d \neq 0$). Therefore, one can coarsely estimate the effective blockade radius at this value. The black curve denotes the case when turning off TBD, i.e., $\Gamma_6 = 0$ while others correspond to the values of $\log_2(\Gamma_6/C_6)$ marked by relevant symbols as shown in (a) (from 2^1 to 2^7). In the calculation, we have used $\Delta_p = 0.3$ MHz and $\Delta_d = -0.35$ MHz which satisfy $\Delta_p + \Delta_d \simeq 0$. $\Omega_p/2\pi = 0.5$ MHz. (b) Effective blockade radius R_b . R_b is increased with respect to the vdW induced blockade radius R_0 when $\Gamma_6 > 0$. The effective blockade radius can be calculated using Eq. (4). The symbols come from data determined from the second order correlation function. Other parameters are the same as in Fig. 2a.

due to stronger energy shift by vdW interactions [21, 49]. On the other hand, the transmission decreases with increasing Γ_6 if one fixes Ω_p .

V. PHOTON-PHOTON CORRELATION AND TBD ENHANCED EXCITATION BLOCKADE

We first present spatial distribution of the correlation function $g_p(R)$ at the EIT resonance $\Delta_p = 0$, shown in Fig. 3b. Without the TBD (dashed curve in Fig. 3b), the correlation function $g_p(R)$ increases from zero at short distances to a peak value, then decays slowly and saturates at a constant value. The smaller value of the correlation function illustrates the photon-photon anti-bunching, resulted from the strong vdW interactions [21, 49]. When turning on the TBD, the correlation function changes quantitatively as a function of distance R . At short distances the correlation function becomes

larger, i.e. probabilities of exciting two Rydberg atoms increase. At intermediate distances, the correlation function exhibits a narrow plateau at around $R_p \sim R_0/2$, then reaches a maximal value. Though maximal values of the correlation function decrease slightly with increasing Γ_6 , they all saturate at very similar values when $R \rightarrow \infty$, where neither TBD nor vdW interactions is important.

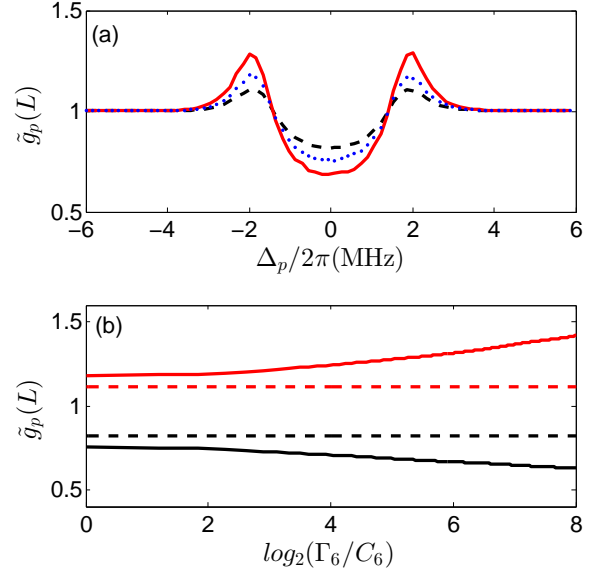


FIG. 4: (Color online) (a) Second-order correlation function $\tilde{g}_p(L)$ versus the probe detuning Δ_p/π for TBD rate $\Gamma_6 = 0$ (dashed), $\Gamma_6 = C_6$ (dotted) and $\Gamma_6 = 32C_6$ (solid). (b) Dependence of the second-order correlation function $\tilde{g}_p(L)$ on the TBD rate Γ_6 when $\Delta_p/2\pi = 0.0$ MHz (black solid) and $\Delta_p/2\pi = 2.0$ MHz (red solid). The dashed black curve ($\Delta_p/2\pi = 0.0$ MHz) and dashed red curve ($\Delta_p/2\pi = 2.0$ MHz) denote the TBD rate $\Gamma_6 = 0$. Other parameters are the same as in Fig. 2a.

The dependence of the correlation function on photon-photon distance R provides valuable information on the blockade radius. As shown in previous section, the modified transmission can be largely explained by examining the respective blockade radius R_b . From Fig. 3b, the TBD has an additive effect on top of the vdW interaction, i.e. increases the blockade radius. The distance when the correlation function is maximal can be assigned as the blockade radius. As a result, we would expect the blockade radius increases with increasing Γ_6 [see also Eq. (4)]. As shown in Fig. 3b, the blockade radius determined from the correlation function is consistent with the analytical prediction Eq. (4).

The TBD enlarged blockade volume will directly affect the light transmission when more atoms are blocked from Rydberg excitation. Here we calculate the number N_a of blocked atoms. Using Eq. (4) we obtain $N_a = 4\pi\rho R_b^3/3 = 4\pi\rho R_0^3 \sqrt{1 - i\Gamma_6/2C_6}/3$. On the other hand, the number N_{SA} of superatoms reduces when the blockade radius

increases with a fixed total volume, see Fig. 3d. For our one dimensional model, we can find the number of superatoms to be $N_{SA} = L/R_b$. As a result, the total number of blockade atoms $\bar{N}_a = N_{SA}N_a = 4\pi L\rho R_b^2/3$, which is proportional to R_b^2 . This indicates that more atoms will be blocked from Rydberg excitation when we increase Γ_6 . This conclusion is consistent with the result shown in Sec. IV (see Fig. 2).

The correlation function exhibits nontrivial dependence on the TBD. To illustrate this, we calculate the normalized correlation function $\tilde{g}_p(L) = g_p(L)/g_p(0)$ at the exist of the medium, shown in Fig. 4a. In the EIT window, $\tilde{g}_p(L)$ becomes smaller when we turn on the TBD. Increasing the rate Γ_6 , the value of the correlation decrease (see Fig. 4a and Fig. 4b). Note that the transmission is large (Fig. 2a) even though the photon is strongly anti-bunched. In contrast, $\tilde{g}_p(L)$ is enhanced by the TBD outside the EIT window $|\Delta_p| > \Omega_d^2/\gamma_e$. We obtain maximal values of the correlation function around the Autler-Townes doublet $\Delta_p \approx \pm\Omega_d$. Increasing the rate Γ_6 , the bunching is also increased (see Fig. 4c). We shall point out that the transmission is smallest at the Autler-Townes doublet. When the photon flux is low, it becomes difficult to measure the TBD amplified bunching.

VI. CONCLUSIONS

In summary, we have studied EIT in a one-dimensional gas of three level ladder-type cold atoms involving highly excited Rydberg states. In this model, each pair of atoms does not only experience the long-range vdW interactions but also the nonlocal two-body dephasing. We show that the TBD can enlarge the effective blockade radius. Through numerical calculations, we demonstrate that in the EIT window, the TBD enhanced blockade effect and gives rise to weaker transmission and stronger

photon-photon anti-bunching. Outside the EIT window, the transmission is hardly affected by the TBD. However, we find that the photon bunching is amplified around the Autler-Townes doublet.

Our work opens new questions in the study of Rydberg EIT. In the present work, we focused on stationary states of extremely long light pulses at zero temperature. It is worth studying how the combination of TBD and vdW interactions will affect propagating dynamics of short light pulses. Rydberg excitation experiments are typically done at finite temperatures. An immediate question here is to study how Rydberg EIT is modified by the presence of TBD at finite temperatures. In Rydberg D -state [66] two-body exchange interactions are typically present. Hence it is interesting how the spin flip-flop interactions are affected by the TBD. It is thus interesting to address these emerging, experimentally relevant questions.

Acknowledgments

D.Y acknowledges support from the National Natural Science Foundation of China (NSFC) Grants No. 11204019 and No. 11874004, the "Spring Sunshine" Plan Foundation of Ministry of Education of China Grant No. Z2017030, the Foundation of Education Department of Jilin Province Grant No. GH16102, and the China Scholarship Council (CSC) Grant No. 201707535012. Z.B acknowledges support from the NSFC Grant No. 11847221, the Shanghai Sailing Program Grant No. 18YF1407100, the China Postdoctoral Science Foundation Grant No. 2017M620140 and the International Postdoctoral Exchange Fellowship Program Grant No. 20180040. W.L. acknowledges support from the UKIERI-UGC Thematic Partnership No. IND/CONT/G/16-17/73, EP-SRC Grant No. EP/M014266/1 and EP/R04340X/1, and support from the University of Nottingham.

[1] S. E. Harris, J. E. Field, and A. Imamoglu, Phys. Rev. Lett. **64**, 1107 (1990).
[2] K.-J. Boller, A. Imamoglu, and S. E. Harris, Phys. Rev. Lett. **66**, 2593 (1991).
[3] M. Fleischhauer, A. Imamoglu, and J. P. Marangos, Rev. Mod. Phys. **77**, 633 (2005).
[4] C. Liu, Z. Dutton, C. H. Behroozi and L. V. Hau, Nature (London) **409**, 490 (2001).
[5] M. D. Lukin, Rev. Mod. Phys. **75**, 457 (2003).
[6] T. Chaneliere, D. N. Matsukevich, S. D. Jenkins, S.-Y. Lan, T. A. B. Kennedy, and A. Kuzmich, Nature (London) **438**, 833 (2005).
[7] J. Appel, E. Figueroa, D. Korytov, M. Lobino, and A. I. Lvovsky, Phys. Rev. Lett. **100**, 093602 (2008).
[8] A. I. Lvovsky, B. C. Sanders, and W. Tittel, Nat. Photonics **3**, 706 (2009).
[9] M. Paternostro and M. S. Kim, B. S. Ham, Phys. Rev. A **67**, 023811 (2003).
[10] M. G. Payne and L. Deng, Phys. Rev. Lett. **91**, 123602 (2003).
[11] C. Ottaviani, D. Vitali, M. Artoni, F. Cataliotti, and P. Tombesi, Phys. Rev. Lett. **90**, 197902 (2003).
[12] D. Petrosyan, J. Opt. B **7**, S141 (2005).
[13] A. V. Gorshkov, R. Nath and T. Pohl, Phys. Rev. Lett. **110**, 153601 (2013).
[14] L. Yang, B. He, J.-H. Wu, Z. Y. Zhang, and M. Xiao, Optica **3**, 1095 (2016).
[15] O. Firstenberg, C. S. Adams, and S. Hofferber, J. Phys. B: At. Mol. Opt. Phys. **49**, 152003 (2016).
[16] M. Saffman and T. G. Walker, Phys. Rev. A **66**, 065403 (2002).
[17] T. G. Walker, Nature **488**, 39 (2012).
[18] M. M. Müller, A. Kölle, R. Löw, T. Pfau, T. Calarco, and S. Montangero, Phys. Rev. A **87**, 053412 (2013).
[19] T. Peyronel, O. Firstenberg, Q.-Y. Liang, S. Hofferberth, A. V. Gorshkov, T. Pohl, M. D. Lukin, and V. Vuletic,

Nature (London) **488**, 57 (2012)

[20] J. Honer, R. Löw, H. Weimer, T. Pfau, and H. P. Büchler, Phys. Rev. Lett. **107**, 093601 (2011).

[21] A. V. Gorshkov, J. Otterbach, M. Fleischhauer, T. Pohl and M. D. Lukin, Phys. Rev. Lett. **107**, 133602 (2011).

[22] H. Gorniaczyk, C. Tresp, J. Schmidt, H. Fedder and S. Hofferberth, Phys. Rev. Lett. **113**, 053601 (2014).

[23] D. Tiarks, S. Baur, K. Schneider, S. Dürr and G. Rempe, Phys. Rev. Lett. **113** 053602 (2014).

[24] W. Chen, K. M. Beck, R. Bücker, M. Gullans, M. D. Lukin, H. Tanji-Suzuki and V. Vuletić, Science **341**, 768 (2013).

[25] S. Baur, D. Tiarks, G. Rempe and S. Dürr, Phys. Rev. Lett. **112**, 073901 (2014).

[26] I. Friedler, G. Kurizki, and D. Petrosyan, Phys. Rev. A **71**, 023803 (2005).

[27] D. Paredes-Barato and C. S. Adams, Phys. Rev. Lett. **112** 040501 (2014).

[28] V. Bendkowsky, B. Butscher, J. Nipper, J. B. Balewski, J. P. Shaffer, R. Löw, and T. Pfau. Phys. Rev. Lett. **105**, 163201 (2010).

[29] Q.-Y. Liang, A. V. Venkatramani, S. H. Cantu, T. L. Nicholson, M. J. Gullans, A. V. Gorshkov, J. D. Thompson, C. Chin, M. D. Lukin, and V. Vuletic, Science **359**, 783 (2018)

[30] M. Saffman, T. G. Walker and K. Mølmer, Rev. Mod. Phys **82**, 2313 (2010).

[31] K. J. Weatherill, J. D. Pritchard, R. P. Abel, M. G. Bason, A. K. Mohapatra, and C. S. Adams, J. Phys. B: At. Mol. Opt. Phys. **41**, 201002 (2008).

[32] J. D. Pritchard, D. Maxwell, A. Gauguet, K. J. Weatherill, M. P. A. Jones, and C. S. Adams, Phys. Rev. Lett. **105**, 193603 (2010).

[33] J. D. Pritchard, A. Gauguet, K. J. Weatherill, and C. S. Adams, J. Phys. B: At. Mol. Opt. Phys. **44**, 184019 (2011).

[34] J. Reslen, J. Phys. B: At. Mol. Opt. Phys. **44**, 195505 (2011).

[35] C. Ates, S. Sevinçli, and T. Pohl, Phys. Rev. A **83**, 041802(R) (2011).

[36] D. Yan, Y.-M. Liu, Q.-Q. Bao, C.-B. Fu, and J.-H. Wu, Phys. Rev. A **86**, 023828 (2012).

[37] D. Yan, C.-L. Cui, Y.-M. Liu, L.-J. Song, and J.-H. Wu, Phys. Rev. A **87**, 023827 (2013).

[38] H. H. Jen and Daw-Wei Wang, Phys. Rev. A **87**, 061802(R) (2013).

[39] M. Gärttner and J. Evers, Phys. Rev. A **88**, 033417 (2013).

[40] J. Stanojevic, V. Parigi, E. Bimbard, A. Ourjoumtsev, and P. Grangier, Phys. Rev. A **88**, 053845 (2013)

[41] Y.-M. Liu, D. Yan, X.-D. Tian, C.-L. Cui, and J.-H. Wu, Phys. Rev. A **89**, 033839 (2014).

[42] H.-Z. Wu, M.-M. Bian, L.-T. Shen, R.-X. Chen, Z.-B. Yang, and S.-B. Zheng, Phys. Rev. A **90**, 045801 (2014).

[43] M. Gärttner, S. Whitlock, D. W. Schonleber, and J. Evers, Phys. Rev. Lett. **113**, 233002 (2014).

[44] G. W. Lin, Y. H. Qi, X. M. Lin, Y. P. Niu, and S. Q. Gong, Phys. Rev. A **92**, 043842 (2015).

[45] S. X. Bao, H. Zhang, J. Zhou, L. J. Zhang, J. M. Zhao, L. T. Xiao, and S. T. Jia, Phys. Rev. A **94**, 043822 (2016).

[46] J. S. Han, T. Vogt, and W. H. Li, Phys. Rev. A **94**, 043806 (2016).

[47] W. C. Xu and B. DeMarco, Phys. Rev. A **93**, 011801(R) (2016).

[48] Q. Zhang Z. Y. Bai, and G. X. Huang, Phys. Rev. A **97**, 043821 (2018).

[49] D. Petrosyan, J. Otterbach, and M. Fleischhauer, Phys. Rev. Lett. **107**, 213601 (2011).

[50] W. Li, D. Viscor, S. Hofferberth, and I. Lesanovsky, Phys. Rev. Lett. **112**, 243601 (2014).

[51] D. Cano and J. Fortagh, Phys. Rev. A **89**, 043413 (2014).

[52] Y.-M. Liu, X.-D. Tian, D. Yan, Y. Zhang, C.-L. Cui and J.-H. Wu, Phys. Rev. A **91**, 043802 (2015).

[53] X.-R. Huang, Z.-X. Ding, C.-S. Hu, L.-T. Shen, W. B. Li, H. Z. Wu, and S.-B. Zheng, Phys. Rev. A **98**, 052324 (2018).

[54] K. Macieszczak, Y. L. Zhou, S. Hofferberth, J. P. Garrahan, W. Li, and I. Lesanovsky, Phys. Rev. A **96**, 043860 (2017).

[55] H. Gorniaczyk, C. Tresp, P. Bienias, A. Paris-Mandoki, W. Li, I. Mirgorodskiy, H. P. Büchler, I. Lesanovsky, and S. Hofferberth, Nat. Commun. **7**, 12480 (2016).

[56] D. Viscor, W. Li, and I. Lesanovsky, New J. Phys. **17**, 033007 (2015).

[57] M. O. Scully and M. S. Zubairy, **Quantum Optics** (Cambridge University Press, Cambridge, England, 1997).

[58] I. Lesanovsky and J. P. Garrahan, Phys. Rev. Lett. **111**, 215305 (2013).

[59] F. Letscher, O. Thomas, T. Niederprüm, M. Fleischhauer, and H. Ott, Phys. Rev. X **7**, 021020 (2017).

[60] S. Ray, S. Sinha, and K. Sengupta, Phys. Rev. A **93**, 033627 (2016).

[61] M. Hoenig, W. Abdussalam, M. Fleischhauer, and T. Pohl, Phys. Rev. A **90**, 021603(R) (2014).

[62] D. W. Schönleber, Martin Gärttner, and Jörg Evers, Phys. Rev. A **89**, 033421 (2014).

[63] J. T. Young, T. Boulier, E. Magnan, E. A. Goldschmidt, R. M. Wilson, S. L. Rolston, J. V. Porto, and A. V. Gorshkov, Phys. Rev. A **97**, 023424 (2018).

[64] T. Wang, S. F. Yelin, R. Côté, E. E. Eyler, S. M. Farooqi, P. L. Gould, M. Koštrun, D. Tong, and D. Vrinceanu, Phys. Rev. A **75**, 033802 (2007).

[65] D. D. Grimes, S. L. Coy, T. J. Barnum, Y. Zhou, S. F. Yelin, and R. W. Field, Phys. Rev. A **95**, 043818 (2017).

[66] C. Tresp, P. Bienias, S. Web er, H. Gorniaczyk, I. Mirgorodskiy, H. P. Büchler, and S. Hofferberth, Phys. Rev. Lett. **115**, 083602 (2015).

[67] B. P. Venkatesh, M. L. Juan, and O. Romero-Isart, Phys. Rev. Lett. **120**, 033602 (2018).

[68] Y.-M. Liu, X.-D. Tian, X. Wang, D. Yan, and J.-H. Wu, Opt. Lett. **41**, 408 (2016).

[69] J. Qian, X.-D. Zhao, L. Zhou, and W. P. Zhang, Phys. Rev. A **88**, 033422 (2013).

[70] K. Mølmer, Y. Castin, and J. Dalibard, J. Opt. Soc. Am. B **10**, 524 (1993).